

# Design of Multi-channel Fringing Electric Field Sensors for Imaging – Part II: Numerical Examples

X. B. Li, C. Kato, A. S. Zyuzin, and A. V. Mamishev  
Sensors, Energy, and Automation Laboratory  
Department of Electrical Engineering  
University of Washington  
Campus Box 352500, Seattle, WA 98195-2500 USA  
shellyli@u.washington.edu

**Abstract:** Two concentric-ring fringing electric field (FEF) sensors are designed for dielectrometry measurement of round samples, as a specific example to further illustrate the design principles for FEF sensors introduced in part I of the paper. Finite element simulations are carried out to analyze and compare such sensor performance characteristics as signal strength and penetration depth. The effects of changes in sensor substrate thickness and shielding electrode width are also evaluated. Simulation results show a clear dependence between these design parameters and sensor performance.

## INTRODUCTION

Figures of merit, such as penetration depth and signal strength, are often used to evaluate the performance of fringing electric field sensors (FEF). These performance characteristics are determined, to a great extent, by the geometry of the sensor. The general design principles are provided in Part 1 of this paper. In this second part, a specific design example is introduced to illustrate the effects of sensor geometry on the penetration depth and signal strength of FEF sensors.

As shown in Part I of the paper, FEF sensors of fixed size are subject to a fundamental trade-off between penetration depth and signal strength: increase in one reduces the other. In this paper, two concentric ring FEF sensors are presented. These sensors are designed for measuring moisture content in cookie dough [1]. This application is driven by the need of food manufacturers to have online real-time control of product properties during the manufacturing process. The second sensor is an improved design based of the first sensor, where shielding electrodes are added to achieve higher penetration depth. The performance of the two sensors is compared using finite element simulations. Sensor signal strength is evaluated through absolute sensor terminal capacitance and penetration depth is evaluated through normalized capacitance.

## TWO CONCENTRIC FEF SENSOR DESIGNS

Figure 1 shows a concentric sensor head designed for measuring moisture content in cookie dough samples. The black ink represents the conductive layer, and the white space represents the insulating substrate beneath. The sensor can be configured as a two-channel FEF sensor, by using the middle electrode as the driving electrode and the other two electrodes as the sensing electrodes. Each sensing electrode needs individual shielding electrodes if the open voltage

measurement scheme is to be used. The readers who need understanding of different measurement schemes used for this type of sensors are referred to [2].

The solution for the Laplace equation of the fringing field concentric sensor geometry is:

$$\phi(r, z) = J_0(\beta r) \left( c_1 e^{-\beta z} + c_2 e^{+\beta z} \right) \quad (1)$$

where  $\phi$  denotes electric potential,  $r$  refers to the radial coordinate on the horizontal plane,  $z$  corresponds to the vertical coordinate,  $J_0$  is the zero order Bessel function of the first kind, and  $\beta$  is a scaling constant such that  $\beta r$  is one of the zeros of  $J_0$  [3].

The spatial wavelength of this design is 8 mm. The sensor penetration depth  $\gamma_{3\%}$  is roughly one third of the wavelength, in other words, it is about 2.5 mm. This is insufficient for measuring most cookie products. Therefore, the penetration depth needs to be increased.

Figure 2 shows an improved design where shielding electrodes are added between the driving and the sensing electrodes to increase the penetration depth. The mechanism of this approach is illustrated in Figure 3. Without shielding electrodes, the backplane draws electric field lines downwards. The shielding electrodes are used to counteract this effect by pushing the electric field lines upward. This increases the penetration depth of the sensor. It should be noted that a short-circuit measurement scheme is more appropriate for the second sensor design, because the upper layer shielding electrodes should be kept at the potential of the respective sensing electrodes. Placement between the sensing electrodes creates an ambiguity, which is resolved by placing all shielding and sensing electrodes at the same zero potential.

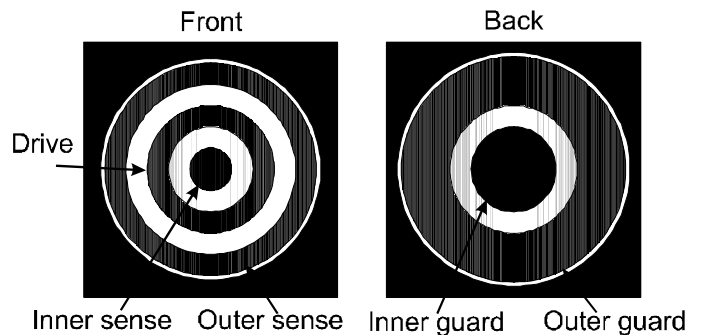


Figure 1. Top-down view of a concentric fringing electric field sensor head.

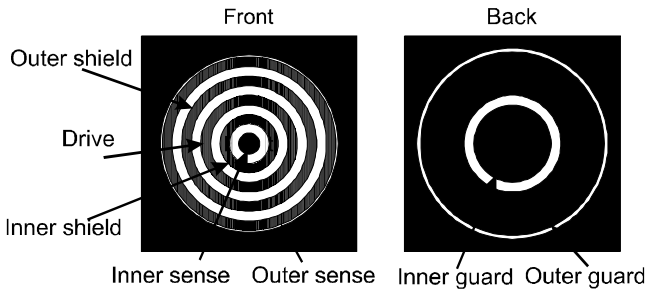


Figure 2. Top-down view of a concentric fringing field sensor head with additional shielding electrodes between the driving and the sensing electrodes.

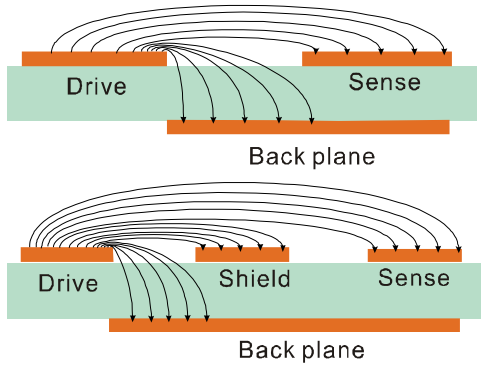


Figure 3. Illustration of the effect of the additional shielding electrodes.

## FINITE ELEMENT ANALYSIS

The software package Maxwell by Ansoft Corp. was used for the finite element (FE) analysis simulations reported here. Figure 4 and Figure 5 show the layout of the simulation space for the two concentric FEF sensor designs shown in Figure 1 and Figure 2, respectively. Both sensors are analyzed with radial coordinates. The origin in the radial direction is placed at the leftmost lowest point of the simulation space. The driving electrode is set to 6 V and all other electrodes (including the backplane) are set to 0 V. For the simplicity of analysis, the test sample is assumed to have relative dielectric permittivity of 5.0, and the conductivity effects are ignored. Inclusion of conductivity does not fundamentally change the results of this analysis, but it would unnecessarily complicate the discussion.

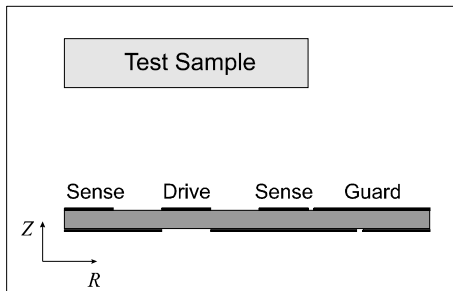


Figure 4. Maxwell simulation layout of a test sample positioned above the concentric FEF sensor of the first design.

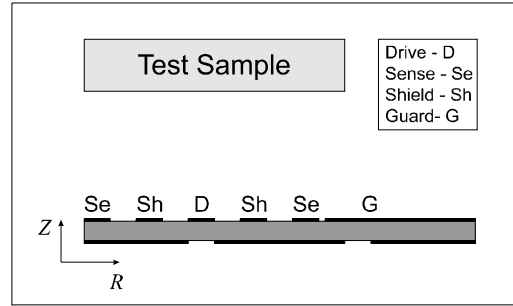


Figure 5. Maxwell simulation layout of a test sample positioned above the shielded concentric FEF sensor of the second design.

Signal strength for each sensor is evaluated based on the absolute terminal capacitance of the sensor. The penetration depth  $\gamma_{3\%}$  is inferred from the normalized terminal capacitance calculations. As specified by the definition in Part I of the paper, penetration depth  $\gamma_{3\%}$  is determined by the distance corresponding to the crossing between the 3% line and the normalized impedance curve.

## THE EFFECT OF THE SHIELDING ELECTRODE

Figure 6 and Figure 7 show respectively the absolute and normalized sensor terminal capacitance value from FE simulations as the distance to the test sample changes. “Sensor 1” refers to the design without shielding electrodes and “Sensor 2” refers to the design with shielding electrodes. For both designs, the outer channel offers greater signal strength than its respective inner channel. The difference in signal strength is caused by the larger sensing area of the outer channel. When compared with the first design, the corresponding channels of the second design do provide greater penetration depth. However, this gain in penetration depth is obtained at the cost of reduced signal strength.

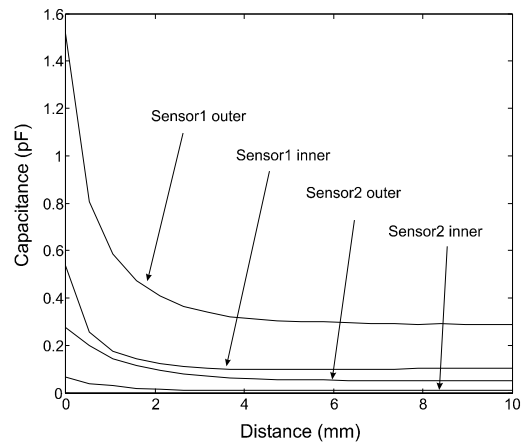


Figure 6. Absolute capacitance value from both sensor designs in the FE simulation.

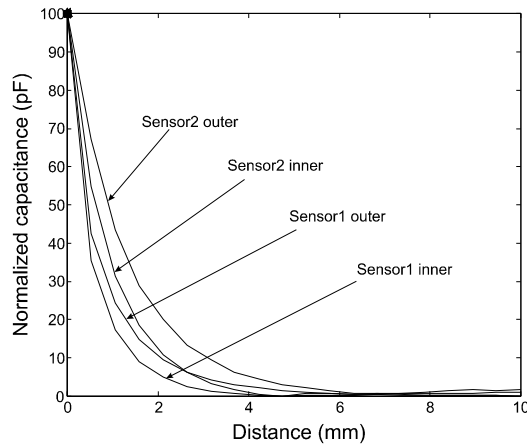
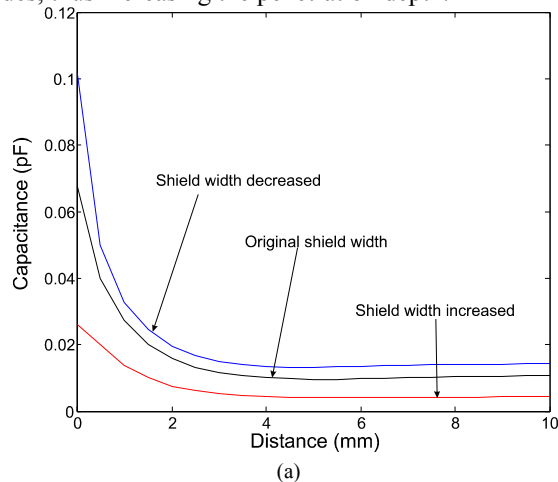


Figure 7. Normalized capacitance value from both sensor designs in the FE simulation.

## THE EFFECT OF SHEILDING ELECTRODE WIDTH

The width of the shielding electrodes is varied in the second design to evaluate its effect on sensor output characteristics. Figure 8 and Figure 9 shows respectively the absolute and normalized capacitance value of the shielded sensor when the shielding electrode width is varied.

The same trend exists for the capacitance value from both the inner and the outer sensing channel: the greater the width of the shielding electrodes the weaker the signal strength and the greater the penetration depth. The result can be interpreted with the help of Figure 3. Increased width of the shielding electrodes draws greater electric field energy from the sensing electrodes, thus decreasing the signal strength; on the other hand, the field lines are pushed further up due to the increased surface area of the shielding electrodes, thus increasing the penetration depth.



## THE EFFECT OF SUBSTRATE THICKNESS

As illustrated in Figure 3, the sensor backplane draws electric field lines away from the sensing electrodes. The closer the back plane is to the driving electrode, the more energy is drawn away. In these designs, the distance between the driving electrode and the backplane is determined by substrate thickness. Therefore, it is important to evaluate the effect of sensor substrate thickness variation on sensor performance.

The thickness of the sensor substrate is varied from 100% to 25% of its original value in a series of FE simulations. Figure 10 shows the absolute capacitance value from the inner channel of the unshielded design. This same trend exists for the capacitance value from both channels of the two sensor designs. The results show that the closer the back plane is to the driving electrode, the weaker the overall sensor signal strength.

In addition to the signal strength, the penetration depth is also affected by change in substrate thickness. The results are shown in Table 1 and Figure 11.

The penetration depth of the first design decreases with increasing substrate thickness. This can again be explained with the illustration in Figure 3. The farther away the backplane is positioned from the electrodes on the top of the substrate, the further down the electric field lines are drawn away from the top electrodes, resulting in a decreased penetration depth. Penetration depth for the second design stays relatively stable against variation in substrate thickness. This is due to the existence of the shielding electrodes. There again exists a trade-off between sensor penetration depth and signal strength: for stronger signal strength, it is desirable to have a thicker substrate, but this decreases the penetration depth of the sensor.

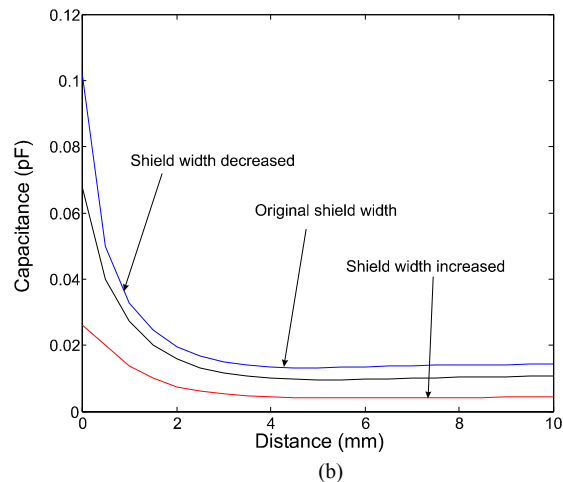


Figure 8. The effect of change in shielding electrode width on the signal strength of the (a) inner sensing channel and (b) outer sensing channel of the shielded sensor. The results show that the sensor signal strength decreases with increasing width of the shielding electrodes.

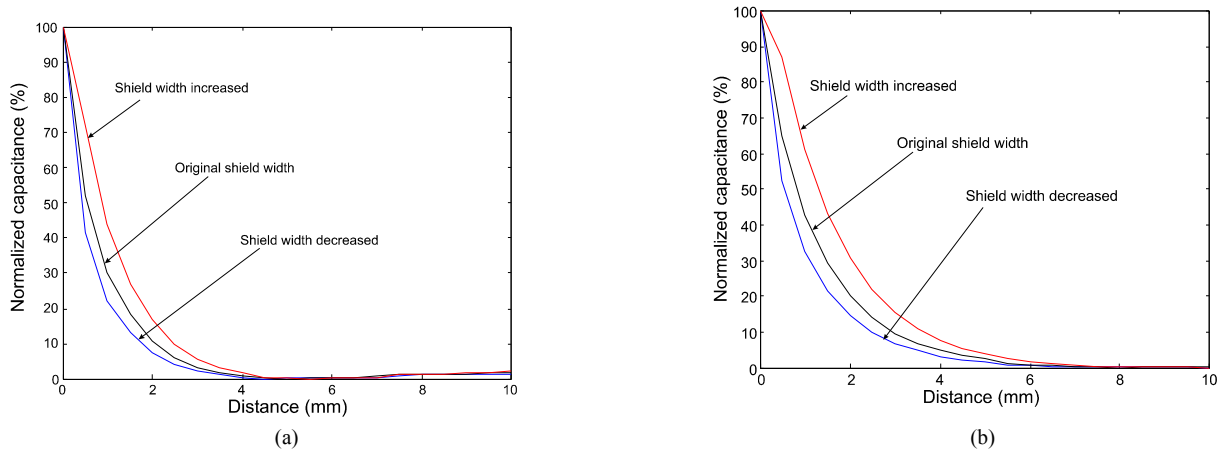


Figure 9. The effect of change in shielding electrode width on the penetration depths of the (a) inner sensing channel and (b) outer sensing channel of the shielded sensor. The results show that the sensor penetration depth increases with increasing width of the shielding electrodes.

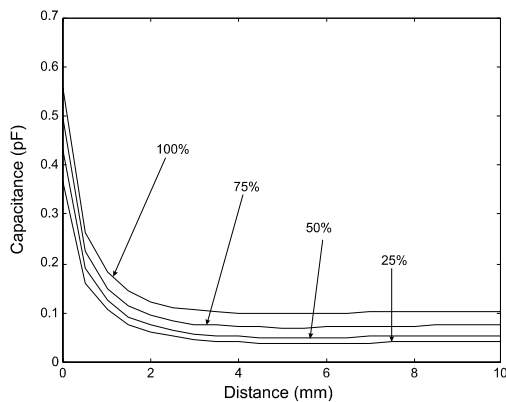


Figure 10. Absolute capacitance value of the inner channel of the unshielded sensor with different substrate thickness.

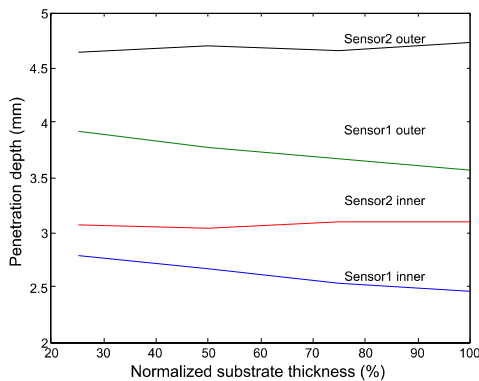


Figure 11. The effect of change in substrate thickness on sensor penetration depth.

**Table 1**  
Penetration Depths (mm) of the Concentric Sensor Designs with Varying Substrate Thickness  $d$ .

$d$	Inner1	Outer1	Inner1	Outer2
25%	2.78	3.91	3.06	4.63
50%	2.67	3.77	3.04	4.69
75%	2.54	3.67	3.09	4.66
100%	2.47	3.57	3.10	4.72

## CONCLUSIONS

Comparative performance analysis of two concentric FEF sensor designs is conducted in this paper. The effect of additional shielding electrode is analyzed through finite element simulations. In addition, the effects of sensor substrate thickness and shielding electrode width are evaluated. The discussion is focused on sensor signal strength, penetration depth, and the trade-off between these two factors. The simulation results demonstrate the effects of sensor geometry on its performance. These results provide insights into the design process of FEF sensors.

## ACKNOWLEDGEMENTS

This work is supported by the Center for Process Analytical Chemistry (University of Washington), the Air Force Office of Scientific Research (AFSOR) grant F49620-02-1-0370, and by the National Science Foundation grant No. ECS-9523128. The author is especially thankful to Sam Larson and Kelly Yedinak (University of Washington) for fabricating the sensor and running some of the finite element simulations. Additionally, the donation of the Maxwell software by Ansoft Corp. is gratefully acknowledged.

## REFERENCES

- [1] X. Li, A. S. Zyuzin, and A. V. Mamishev, "Measuring Moisture Content in Cookies Using Dielectric Spectroscopy," *2003 Annual Report Conference on Electrical Insulation and Dielectric Phenomena*, vol. 1, 2003, pp. 459-462.
- [2] A. V. Mamishev, K. Sundara-Rajan, F. Yang, Y. Q. Du, and M. Zahn, "Interdigital Sensors and Transducers," *Proceedings of the IEEE*, vol. 92, no. 5, pp. 808-845, May 2004.
- [3] I. C. Shay and M. Zahn, "Cylindrical Geometry Electroquasistatic Dielectrometry Sensors," *IEEE Conference on Electrical Insulation and Dielectric Phenomena*, 2002, pp. 126-129.